*J. Phycol.* **35,** 270–279 (1999)

# HETEROGENEITY OF OXYGEN PRODUCTION AND CONSUMPTION IN A PHOTOSYNTHETIC MICROBIAL MAT AS STUDIED BY PLANAR OPTODES[1]

*Ronnie Nøhr Glud*[2] *and Michael Kühl*

University of Copenhagen, Marine Biological Laboratory, Strandpromenaden 5, DK-3000 Helsingør, Denmark

*Oliver Kohls*

Max Planck Institute for Marine Microbiology, Microsensor Group, Celsiusstrasse 1, D-28359 Bremen, Germany

*and*

*Niels Birger Ramsing*

University of Aarhus, Institute of Biology, Department of Microbial Ecology, Ny Munkegade bgn. 550, DK-8000 Aarhus C. Denmark

**By applying planar optodes and imaging techniques to a benthic photosynthetic mat, we demonstrated an extensive vertical and horizontal variation in $O_2$ concentrations, $O_2$ consumption, and $O_2$ production. In light, the oxic zone could be divided into three horizons: 1) an upper zone dominated by diatoms that had a moderate net $O_2$ production, 2) another zone dominated by Microcoleus-like cyanobacteria with a high net $O_2$ production, and 3) a lower zone with disintegrating microalgae and cyanobacteria with a high $O_2$ consumption rate. From the $O_2$ images, the net $O_2$ production/consumption was calculated at a spatial resolution of 130 μM. This allowed us to identify microsites with high rates of $O_2$ turnover within the photic zone. Sites with high net $O_2$ consumption ($>1.5$ nmol·cm$^{-3}$·s$^{-1}$) were typically situated next to sites with a relatively high net production ($>2$ nmol·cm$^{-3}$·s$^{-1}$), revealing a mosaic in which the highest $O_2$ consumption sites were surrounded by the highest $O_2$ production sites. This suggested a tight spatial coupling between production and consumption of $O_2$ within the photic zone. Light stimulated the $O_2$ consumption within the photic zone. At irradiances above 400 μmol photons·m$^{-2}$·s$^{-1}$, the stimulated $O_2$ production was almost completely balanced by enhanced $O_2$ consumption at microsites exhibiting net consumption of $O_2$ even at maximum irradiance (578 μmol photons·m$^{-2}$·s$^{-1}$). Our observations strongly supported the idea that light-stimulated respiration was caused by stimulated heterotrophic activity fueled by organic carbon leakage from the phototrophs. Despite microsites with high net $O_2$ consumption, anoxic microniches were not encountered in the investigated mat. Images of gross photosynthetic rates also revealed an extensive horizontal variation in gross rates, with microsites of low or no photosynthesis within the otherwise photic zone. Calculations based on the obtained images revealed that at maximum light (578 μmol photons·m$^{-2}$·s$^{-1}$), 90% of the $O_2$ produced was consumed within the photic zone. The presented data demonstrate the great potential offered by planar optode for studies of benthic photosynthetic communities.**

*Key index words:* **microbial mat; microcoleus; microsensor; optodes; oxygen; photosynthesis; respiration**

In recent decades, benthic photosynthetic communities in sediments and microbial mats have received much attention because of their importance for primary production and nutrient cycling of shallow-water environments (e.g. Colijn and De Jonge 1984, Duarte and Cebrian 1996). Additionally, the presumed resemblance between recent mats and Precambrian stromatolites has stimulated research in C and O cycling within various photosynthetic communities (e.g. Canfield and DesMarais 1993). Photosynthetic mats are characterized by intense $O_2$ dynamic within a <1- to 5-mm-thick surface layer in which the $O_2$ saturation typically varies between 0% and 100% during a daily cycle (e.g. Revsbech et al. 1983). This fluctuation in oxia has a major impact on the biogeochemical cycling and on the ecology of microorganisms and meiofauna living within such communities (e.g. Canfield and DesMarais 1993, Garcia-Pichel et al. 1994, Fenchel and Bernard 1996). The respiratory pathways of most benthic communities are both spatially and temporally coupled to the oxic conditions, and light-stimulated $O_2$ consumption has been encountered in various microbial mats. This has been ascribed to increased $O_2$ penetration depths in light (Epping and Jørgensen 1995), reoxidation of an $O_2$ debt developing in darkness (Fenchel 1998), photorespiration (Glud et al. 1992, Canfield and DesMarais 1993), and enhanced heterotrophic $O_2$ consumption in light (Ludden et al. 1985, Glud et al. 1992, Kühl et al. 1996). Studies of the apparent tight coupling between photosynthesis and various respiratory pathways in benthic communities require techniques with a high spatial and temporal resolution.

Oxygen microelectrodes have been unique tools for describing and exploring the tight spatial and

[1] Received 3 September 1998. Accepted 30 December 1998.
[2] Author for reprint requests; e-mail mblrg@mail.centrum.dk.

temporal coupling between production and consumption of $O_2$ in benthic communities (e.g. Revsbech et al. 1981, 1983, Glud et al. 1992, Epping and Jørgensen 1995, Kühl et al. 1996). Microelectrode studies have also revealed the physical reality and the importance of the diffusive boundary layer (DBL) for microbial mat communities (Jørgensen and Revsbech 1985, Jørgensen and DesMarais 1990). The 0.5- to 1.0-mm-thick DBL is a thin film of water covering benthic communities through which diffusion is the dominant transport mode for solute exchange. The DBL is characterized by a zone with linear solute concentration gradient overlaid by a transition zone where the eddy diffusion gradually increases toward the overlying turbulent water phase (Jørgensen and Revsbech 1985). A fiberoptic $O_2$ microsensor (microoptode) was introduced to aquatic biology by Klimant et al. (1995) as an alternative to microelectrodes. This new sensor is based on the principle of dynamic quenching of an immobilized luminophore by $O_2$ that decreases the luminescent quantum yield (Kautsky 1939). Compared to microelectrodes, the new sensor is much simpler to manufacture, has a superior long-term stability, and has no analyte consumption (Klimant et al. 1995). Despite the high data quality that can be obtained by both types of microsensors, microprofiles represent only a one-dimensional approach measured at single positions, and the results are extrapolated to larger areas. However, microelectrode measurements have also demonstrated that extensive heterogeneity in physical and chemical parameters can exist in benthic photosynthetic mats and that a simple one-dimensional approach might not always be valid (Jørgensen et al. 1983, Jørgensen and DesMarais 1990). To overcome or to describe the heterogeneity in the $O_2$ distribution, $O_2$ consumption and production by measuring multiple microprofiles is an overwhelming and often impossible task.

Recently, planar optodes, a technique capable of resolving the two-dimensional $O_2$ dynamic in benthic communities at a high spatial and temporal resolution, has been introduced to aquatic biogeochemistry (Glud et al. 1996, 1998). To resolve the $O_2$ dynamic in a photosynthetic mat, we applied a planar optode to a cyanobacterial mat. Data resolving the heterogeneous two-dimensional distribution of $O_2$, respiration, and photosynthesis in a mat community are presented and discussed in relation to mat structure, microenvironments, and light-enhanced $O_2$ consumption.

## MATERIALS AND METHODS

*Planar optode.* Planar optodes were made of the $O_2$-quenchable luminophore ruthenium (III)-Tris-4,7-diphenyl-1,10-phena-throline, which absorbs blue light (450 nm) and emits red light with a maximum intensity at 610 nm. Because of the quenching by $O_2$, the intensity of the emitted red light is inversely proportional to the $O_2$ partial pressure experienced by the luminophore (see the following discussion). The luminophore was dissolved in plasticized PVC and applied by knife coating onto a transparent $O_2$-impermeable polyester support foil. To avoid optical interference between the experimental setup and the photosynthetic community, the sensing layer was coated with black silicone for optical isolation (Klimant et al. 1995, Glud et al. 1996). The total thickness of the planar optodes was approximately 220 μM, divided into a 175-μM-thick support foil, 10 μM of immobilized luminophore, and 40 μM of optical isolation. After curing of the silicone, the planar optodes were cut into 25 × 55-mm pieces and then fixed to the inside of a small transparent flume by a layer of colorless silicone (Fig. 1). For details on planar optode fabrication, see Glud et al. (1996).

*Experimental setup.* The investigated 5-cm-thick microbial mat was collected in the hypersaline salt marsh of Um-El-Yums Sabka, Egypt. It consisted of a thin layer of diatoms overgrowing a dense layer of cyanobacteria (*Microcoleus* s.p.). Below the 2-mm-thick *Microcoleus* layer, a distinct white horizon of precipitated carbonate covering a brown layer of disintegrated cells and carbonate grains was observed. The mat was gelatinous and was easily cut into the shape of the rectangular flume (6 × 8 × 20 cm) (Fig. 1). The mat was placed in front of the planar optode and fixed on the three other sides by 2% agar applied at a temperature of 38° C. Subsequently, aerated artificial seawater of 80‰ salinity (equal to *in situ* conditions) was circulated over the mat. It cannot be completely excluded that the sampling procedure affected the microenviroment (e.g. the solute gradients) of the mat transitionally; however, an acclimation period of 24 h was applied prior to any measurements. A circulation pump ensured that the free flow velocity above the mat was kept constant at 0.3 $cm \cdot s^{-1}$ during all the presented experiments. The $O_2$ saturation was kept at 21% by continuous aeration of the brine. The mat sample was illuminated vertically by a fiberoptic halogen lamp equipped with a heat filter and a collimating lens. After the experiments, the downwelling irradiance applied to the mat was quantified by a scalar irradiance meter (Biospherical Instruments, QSL-100) placed over a black light well at the same position as the mat surface during the experiments. Black screens and cloth were used for optical isolation between the flume and the measuring system of the planar optode (Fig. 1). A total of three mat samples were investigated.

The planar optode was excited by a halogen lamp equipped with a blue glass filter (BG 12, Schott). A 60-mm Nikon lens and a long-pass glass filter (OG 570, Schott) were adapted to the CCD camera (Photometrics, CH250L), which recorded the red luminescent light emitted by the planar optode (Fig. 1). The camera was equipped with a Peltier-cooled CCD chip (KAF 1400 1317 × 1035 pixels) and was controlled from a Macintosh Quadra computer. The digital transmission of an image from the camera to the computer took 1.7 s, which determined the maximum frequency by which images could be obtained. Flume, camera, lamps, and filters were fixed in a custom design rack to stabilize the experimental setup against vibrations. Image acquisition was done with the Photometrics camera software, and subsequent calibration and analysis of the obtained images were done with custom software routines and with the publicly available NIH-image Version 1.58 image analysis program (FTP site zippy.nimh.nih.gov).

*Image recording and calibration.* The intensity of the luminescent light emitted by the planar optode was obtained by the CCD camera with a binding factor of two, implying that an average value of only four neighboring pixels was stored. This reduced the original number of pixels to $3.4 \times 10^5$. The images covered 226 $mm^2$ (13.3 × 17.0 mm), and the distribution of the $O_2$ sensitive luminescent light was consequently resolved, horizontally and vertically, at 26 μM spatial resolution. The acquired images were recorded as 12-bit images expressed on a linear gray scale from 0 to 4095.

The relation between the $O_2$ concentration (C) and the luminescent light intensity (I) emitted by the optode was described by a modified Stern-Volmer equation (Klimant et al. 1995):

$$I = I_0\left[\alpha + (1 - \alpha)\left(\frac{1}{1 + K_{SV}C}\right)\right] \quad (1)$$

which was rearranged into:

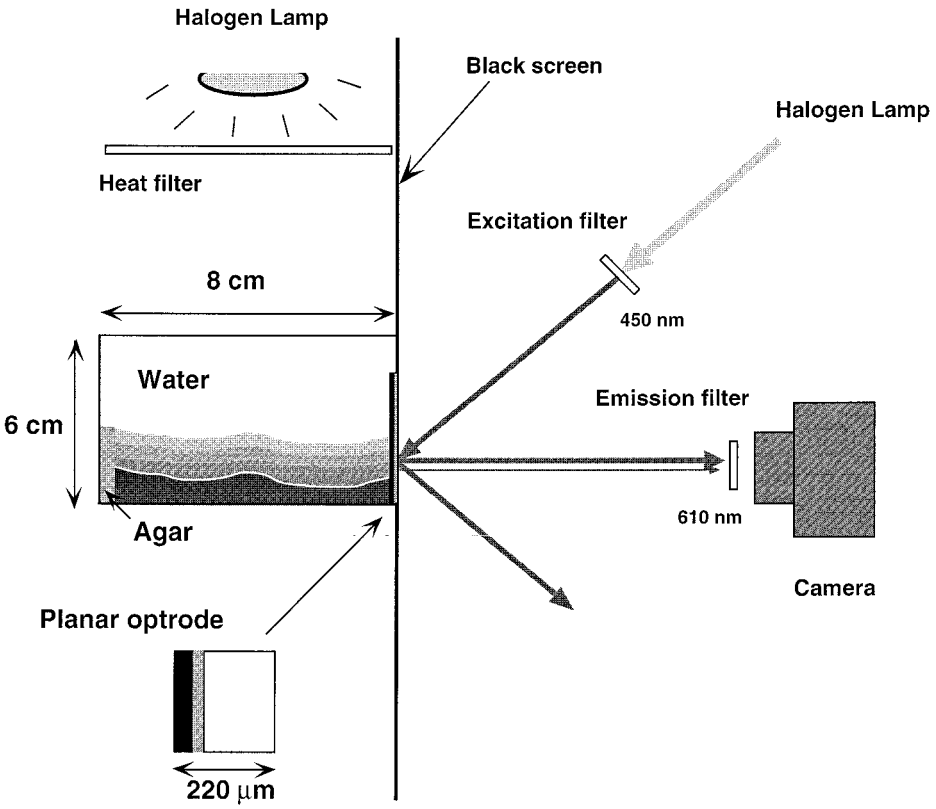


FIG. 1. Schematic drawing of the experimental setup. The water flow direction was perpendicular to the paper. An enlargement of the planar optode is shown at the bottom of the figure.

$$C = \frac{I_0 - I}{K_{SV}(I - I_0\alpha)} \quad (2)$$

where $\alpha$ is the nonquenchable fraction of the luminescence, $I_0$ is the luminescence intensity in the absence of $O_2$, and $K_{SV}$ is a constant expressing the quenching efficiency of the immobilized luminiphore (Stern and Volmer 1919, Klimant et al. 1995). The inhomogeneity of the planar optode and the light field of the excitation beam was too large to assume constancy over the foil area of $\alpha$, $K_{SV}$ or $I_0$. Therefore, an individual three-point calibration of each of the $3.4 \times 10^5$ stored pixel values was performed (for details, see Glud et al. 1996). Calibration images were obtained after the experiments by removing the microbial mat from the sensor foil; subsequently, as the flume was flushed with $N_2$, air, and pure $O_2$, images were acquired. By applying the pixel-dependent values of $\alpha$, $K_{SV}$, and $I_0$ calculated from the calibration images to equation 2, the $O_2$ distribution in images obtained during the experiment could be calculated.

Prior to the calibration procedure, the position of the mat surface was determined by depositing sodium dithionite grains along the wall of the flume while acquiring a series of images. The dithionite grains landed at the surface and reduced any dissolved $O_2$ in their vicinity and appeared as reduced areas on the calibrated images. The mat surface was determined by interconnecting the reduced areas as they first appeared in the series of $O_2$ images (for details, see Glud et al. 1996).

*Measurements of oxygen distribution and gross photosynthesis.* Initially, the irradiance exposed to the microbial mat was increased stepwise from 0 to 578 μmol photons·$m^{-2}$·$s^{-1}$. After each change, we waited approximately 25 min until the $O_2$ distribution reached steady state, as evaluated from a series of images. Subsequently, at each irradiance the gross photosynthesis was estimated by the light–dark-shift technique (Revsbech and Jørgensen 1983, Glud et al. 1992). By this technique, the gross photosynthesis is calculated from the initial decrease of oxygen at a given position after eclipse of the light source, assuming 1) a steady-state $O_2$ distribution before darkening, 2) an identical $O_2$ consumption before and during the light–dark shift, and 3) constant $O_2$ gradients within the community. It has been demonstrated that assumptions 1 and 2 are or can be fulfilled in benthic photosynthetic communities but that assumption 3 requires that the absolutely initial decrease in $O_2$ concentration is used for the calculation (Glud et al. 1992, Lassen et al. 1998). If this is not possible, the measured distribution of activities are smeared out in such a way that peak activities are underestimated and the low activities overestimated. However, the depth-integrated activity will remain unaffected by the dark incubation length during the initial 5 s (Glud et al. 1992, Lassen et al. 1998).

We inserted a black screen between the microbial mat and the light source while images were recorded at maximum frequency (1 image per 1.7 s) for a total of 8.5 s. By simple arithmetic, it was later possible to calculate the rate by which the $O_2$ concentration decreased at each pixel.

## RESULTS AND DISCUSSION

The steady-state $O_2$ distribution within the mat was measured at six different irradiances, of which two are presented in Figure 2A, B. In darkness, the $O_2$ penetration depth along the 17-mm-long transect varied from 1.16 to 2.30 mm, with an average value of 1.51 ± 0.32 mm. At maximum irradiance (578 μmol photons·$m^{-2}$·$s^{-1}$), the average $O_2$ penetration increased to 3.16 ± 0.69 mm, with a minimum and maximum value of 2.50 and 4.09 mm, respectively. The $O_2$ distribution within the oxic zone was heterogeneous, and sites with relatively high and low $O_2$ concentrations could be observed, especially in light (Fig. 2). During the study, we investigated $3 \times 17$-mm transects and did not observe any temporal or permanent anaerobic microniches (anoxic pixels surrounded by oxic pixels).

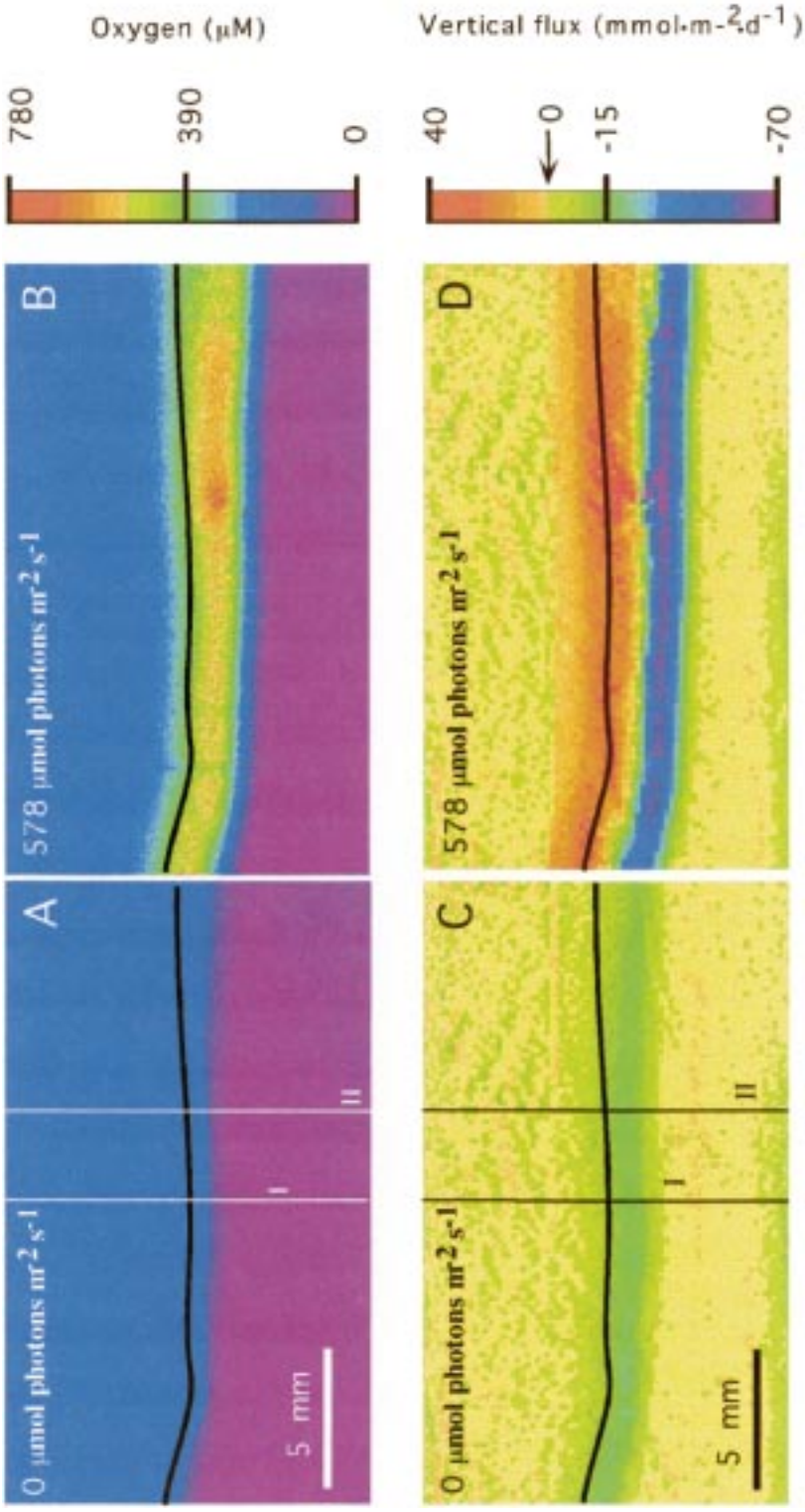


FIG. 2 (A, B) An image of the $O_2$ distribution within a microbial mat in darkness and 578 µmol photons·$m^{-2}$·$s^{-1}$, respectively. (C, D) The vertical diffusive flux calculated from the $O_2$ images above. The wide horizontal line indicates the position of the mat surface, whereas the two thin vertical lines indicate the position of the profiles shown in Figure 3. Scale bar indicates the physical dimensions.

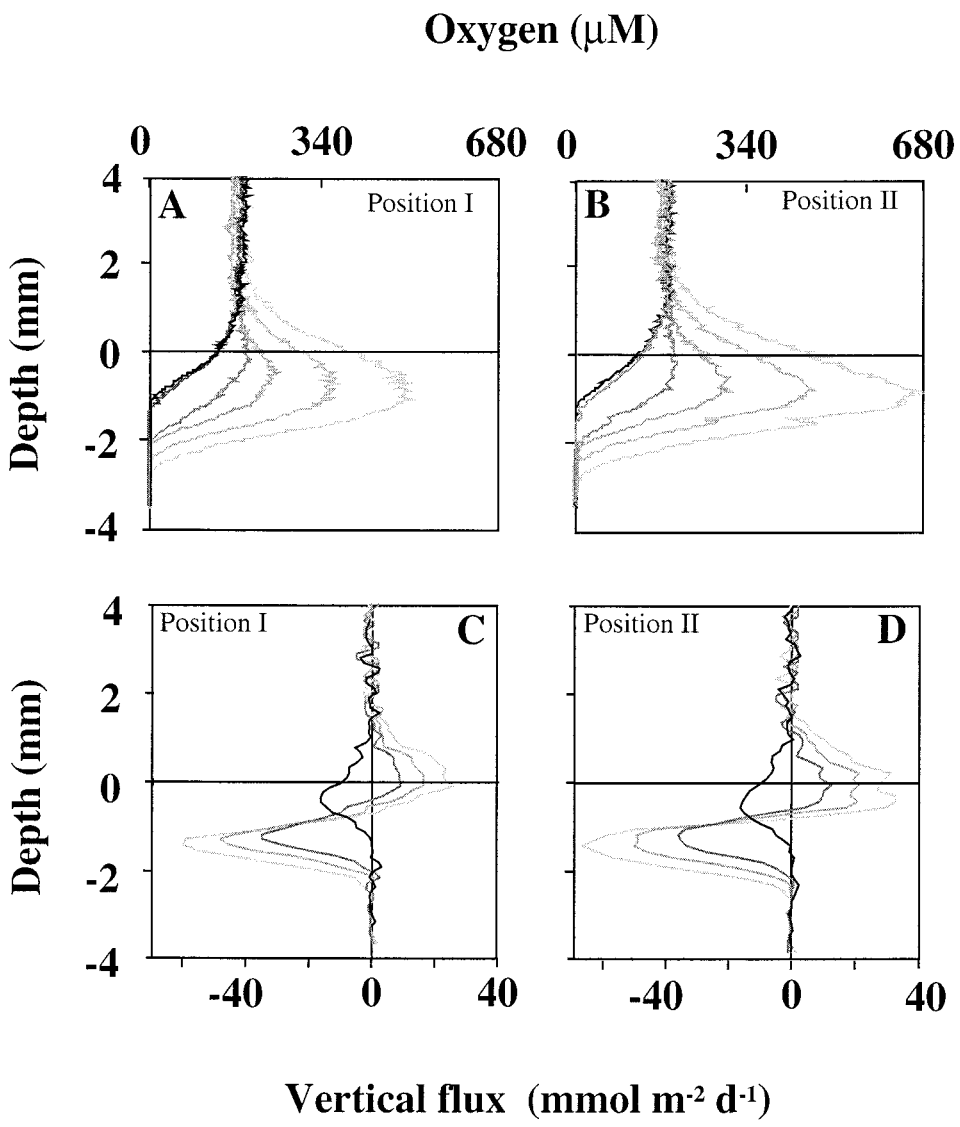


FIG. 3. Oxygen concentration and vertical flux values as a function of irradiance (0, 29, 124, 361, 473, and 578 μmol photons·m$^{-2}$·s$^{-1}$ and flux at 0, 361, 473, and 578 μmol photons·m$^{-2}$·s$^{-1}$) extracted along lines I and II in Figure 2. The tone of gray level indicates the different light intensities at which the profiles were obtained, with the lightest being maximum irradiance and the darkest being complete darkness. The fat horizontal line indicates the position of the mat surface.

The diffusive exchange along the concentration gradients was calculated by applying Ficks first law of diffusion, $J(z) = D_e(z) \cdot (\delta C(z)/\delta z)$, where $D_e$ is the transport coefficient, $C$ the $O_2$ concentration, and $z$ the position (Crank 1983). In the following, a negative flux refers to a net downward flux, whereas a positive flux refers to a net upward flux. It was not possible to determine the transport coefficients within the mat at the scale relevant to our study, so we applied the diffusive transport coefficient of $O_2$ at the experimental conditions ($D_e(z) = 1.83 \times 10^{-5}$ cm$^2$·s$^{-1}$) (Broecker and Peng 1974, Li and Gregory 1974). Performing the calculation on the raw $O_2$ images resulted in an unacceptable level of scatter due to small-scale noise in the original images. As a compromise between reduced scatter and high spatial resolution, the calculations were performed after averaging 25 neighboring pixels, reducing the original number of pixels from $3.4 \times 10^5$ to $13.6 \times 10^3$ and, consequently, reducing the spatial resolution to 130 μM. Despite the heterogeneous $O_2$ distribution within the oxic zone, the horizontal $O_2$ flux was less than 5% of the vertical flux in all instances (data not shown). Figure 2C, D shows the vertical flux in darkness and the maximum irradiance, respectively.

It is visually difficult to separate the values presented in Figure 2, so, as an example, the $O_2$ concentration and the $O_2$ flux at six and four irradiances along the vertical lines indicated in Figure 2A, C are presented as traditional microprofiles in Figure 3. The difference in $O_2$ distribution and flux at the two positions separated by less than 3 mm was significant. The $O_2$ gradient across the DBL immediately above the mat was indistinguishable from linear and reflected how the diffusive $O_2$ uptake in darkness gradually changed into an $O_2$ export as the irradiance was increased (Figs. 2, 3). The mat had a light compensation point (no net exchange across the DBL) at approximately 40 μmol photons·m$^{-2}$·s$^{-1}$. This is comparable to compensation

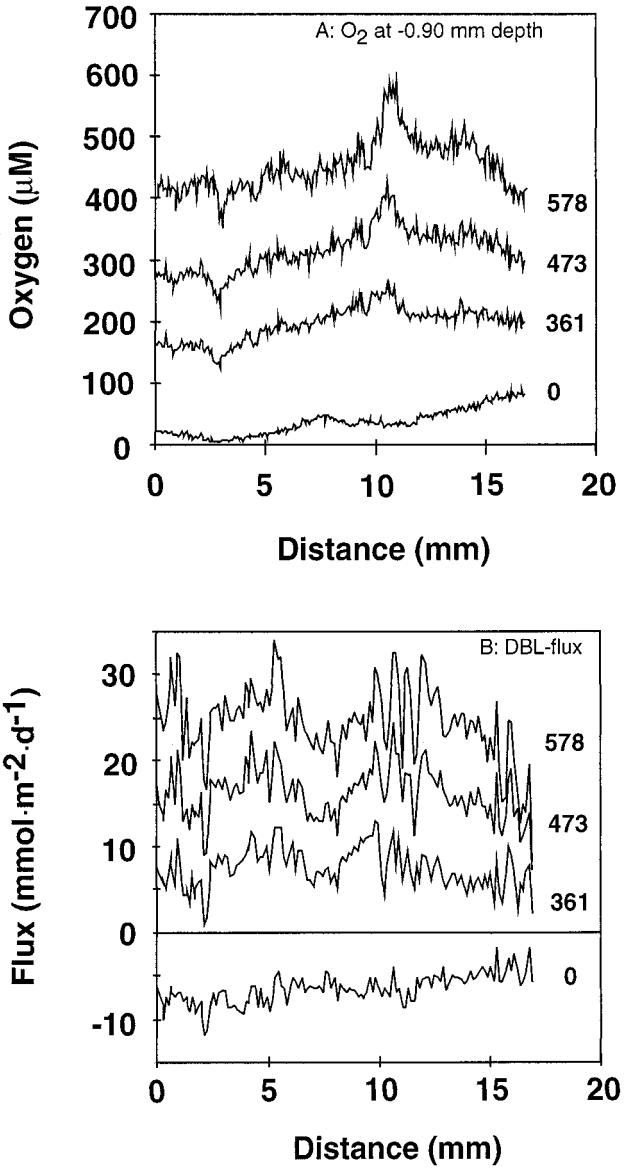


FIG. 4. (A) Oxygen concentration 900 μm below the mat surface at four different irradiances (indicated with numbers in μmol photons·m$^{-2}$·s$^{-1}$). The data were extracted from the $O_2$ images shown in Figure 2A, B and from two additional images (not shown). (B) The vertical flux through the DBL along the investigated transect. Data were extracted from the flux images shown in Figure 2C, D plus two additional images (not shown).

points determined for similar mats investigated by Epping and Jørgensen (1996). Apparently, the thickness of the transition zone between the DBL and the overlying turbulent-water phase increased as the $O_2$ gradients became steeper (Fig. 3). The transition zone is not a hydrodynamically well-defined layer (Jørgensen and Revsbech 1985), but it is to be expected that steeper concentration gradients will make the gradual decrease in eddy diffusion toward the mat surface more visible. However, it is important to notice that a thin film of water with diffusive mediated $O_2$ transport will cover the planar optode in a similar way as the DBL covers the mat surface. The result will be a gradual increase in DBL thickness toward the planar optode fixed at the flume wall. To the extent that the DBL impedes the exchange rate across the interface, the $O_2$ gradient measured along the sensor will be underestimated. The effect is comparable but opposite to the DBL compression imposed by microsensors approaching a mat surface. Here the presence of a sensor also causes an asymmetrical change in the DBL structure but in this case leading to a thinner DBL and thereby an enhanced diffusive exchange at the measuring point (Glud et al. 1994). These effects do not invalidate the techniques, but data are obtained under a changed flow regime as compared to the nondisturbed situation. The vertical flux profiles demonstrated that fluxes are constant just above the mat surface, that they are positive in the upper 800 to 900 μm during light, and that the position for minimum fluxes moved downward with increased irradiance but remained approximately 700 μm above the oxic–anoxic interface (Fig. 3C, D).

The horizontal heterogeneity in concentrations and flux is also demonstrated in Figure 4, in which the $O_2$ concentration along a transect 0.90 mm below the mat surface (Fig. 4A) and the diffusive exchange across the DBL (Fig. 4B) at four different light intensities is shown. At the 3.0-mm lateral position, a local minimum in $O_2$ concentration can be observed in darkness as well as in light, whereas the 10.5-mm position represents a site with local minimum in darkness which turn into a local maximum in light (Fig. 4A). The various responses to light probably reflect the differences in relative abundance of phototrophs and heterotrophs at the various sites (see the following discussion). The diffusive exchange across the interface was highly variable at a given irradiance but on average increased from $-6.5 \pm 1.7$ mmol $O_2 \cdot m^{-2} \cdot day^{-1}$ in darkness to $24.5 \pm 4.3$ mmol $O_2 \cdot m^{-2} \cdot day^{-1}$ at maximum light. Positions from 15 mm and outward showed light saturation at the highest light intensities (Fig. 4B). The downward flux of $O_2$ from the photic zone at maximum light was $58.2 \pm 4.9$ mmol $\cdot m^{-2} \cdot day^{-1}$.

The net activity (photosynthesis minus respiration) was calculated from the original $O_2$ images at a spatial resolution of 130 μM by applying a modified version of Ficks second law of diffusion: $P(z) - R(z) = D_e(z) \bullet (\delta^2 C(z)/\delta z^2)$, where $P$ and $R$ are the photosynthesis and respiration, respectively (Revsbech et al. 1981). At maximum irradiance, the oxic zone could be divided into three horizontal layers, the upper 0.4 mm showing low net $O_2$ production, a depth range from 0.4 to 1.2 mm showing high net $O_2$ production, and a deeper zone showing high net $O_2$ consumption (Fig. 5). The depth horizons coincided with the layers dominated by diatoms, *Microcoleus,* and disintegrating cells, respectively. The photic zone (here defined as the horizon with net

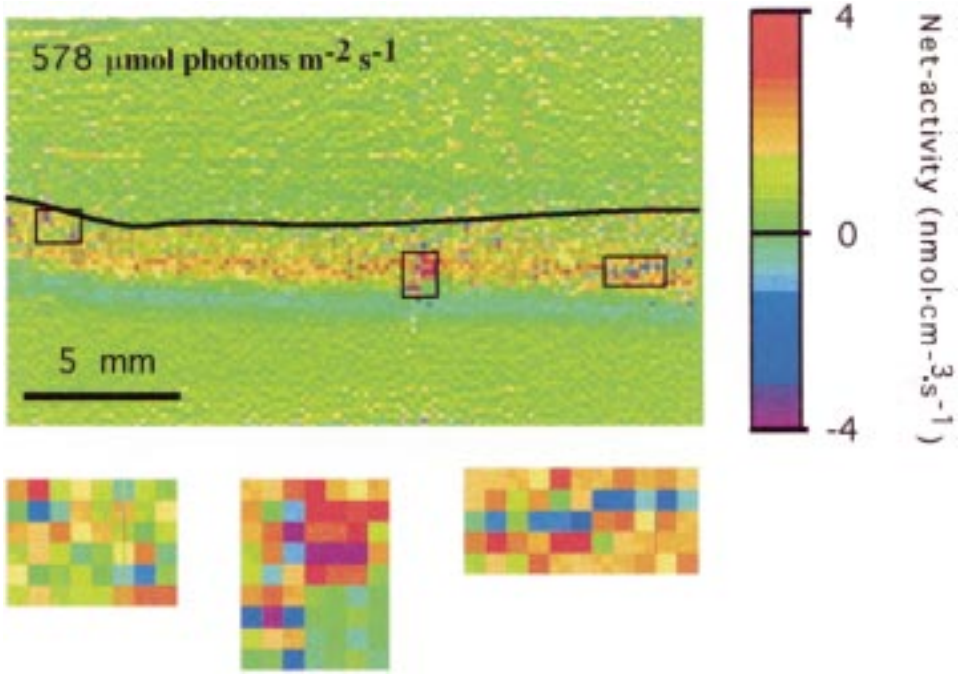


FIG. 5. Net $O_2$ production (positive) and net $O_2$ consumption (negative) within the investigated mat. Scale bar indicates the physical dimensions and the wide horizontal line the position of the mat surface. Three areas indicated in the original images are enlarged (400%) and included in the lower panel.

$O_2$ production) consisted of approximately 1180 pixels, with an average net $O_2$ production of 0.47 ± 0.90 nmol·cm$^{-3}$·s$^{-1}$. Within that zone, only 56 pixels had a net $O_2$ production above 2.0 nmol·cm$^{-3}$·s$^{-1}$, whereas 28 pixels had a $O_2$ consumption higher than 1.5 nmol·cm$^{-3}$·s$^{-1}$, and 86% of the high-consumption pixels (blue/purple) were neighboring high-production pixels (dark red) (Fig. 5). The cooccurence of such pixels was also observed when the calculation was performed at a spatial resolution of 26 µM, but the noise level in such net-activity images was too high to allow further calculation (data not shown).

The observation suggests a tight spatial coupling between sites characterized by high production and sites of high consumption. The net production of $O_2$ increased with increasing irradiance, and above 400 µmol photons·m$^{-2}$·s$^{-1}$, this was associated with

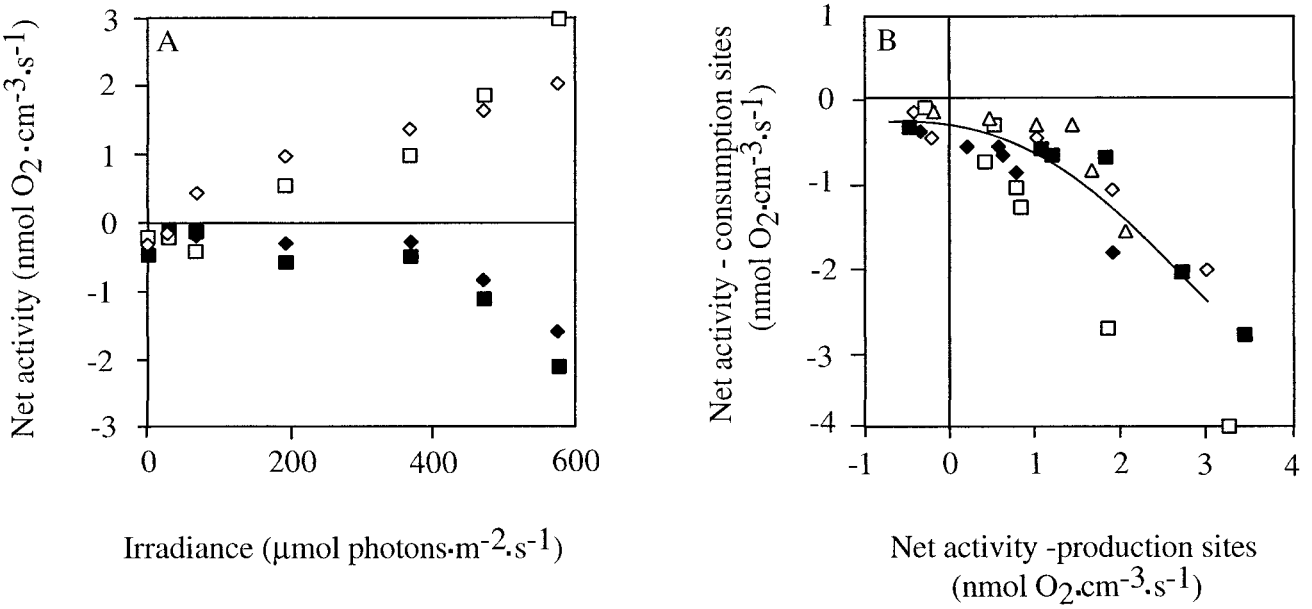


FIG. 6. (A) Net activity of four pixels as a function of irradiance. The squared symbols represent one neighboring pair, whereas the diamonds indicate another pair. Open symbols represent data of the net productive sites, whereas closed symbols refer to values obtained at net consumption sites. (B) Five pairs of neighboring pixels showing net $O_2$ consumption and net $O_2$ production, respectively. The $O_2$ consumption rate by the $O_2$-consuming pixels are plotted as a function of the net $O_2$ production rate of their neighboring pixel.

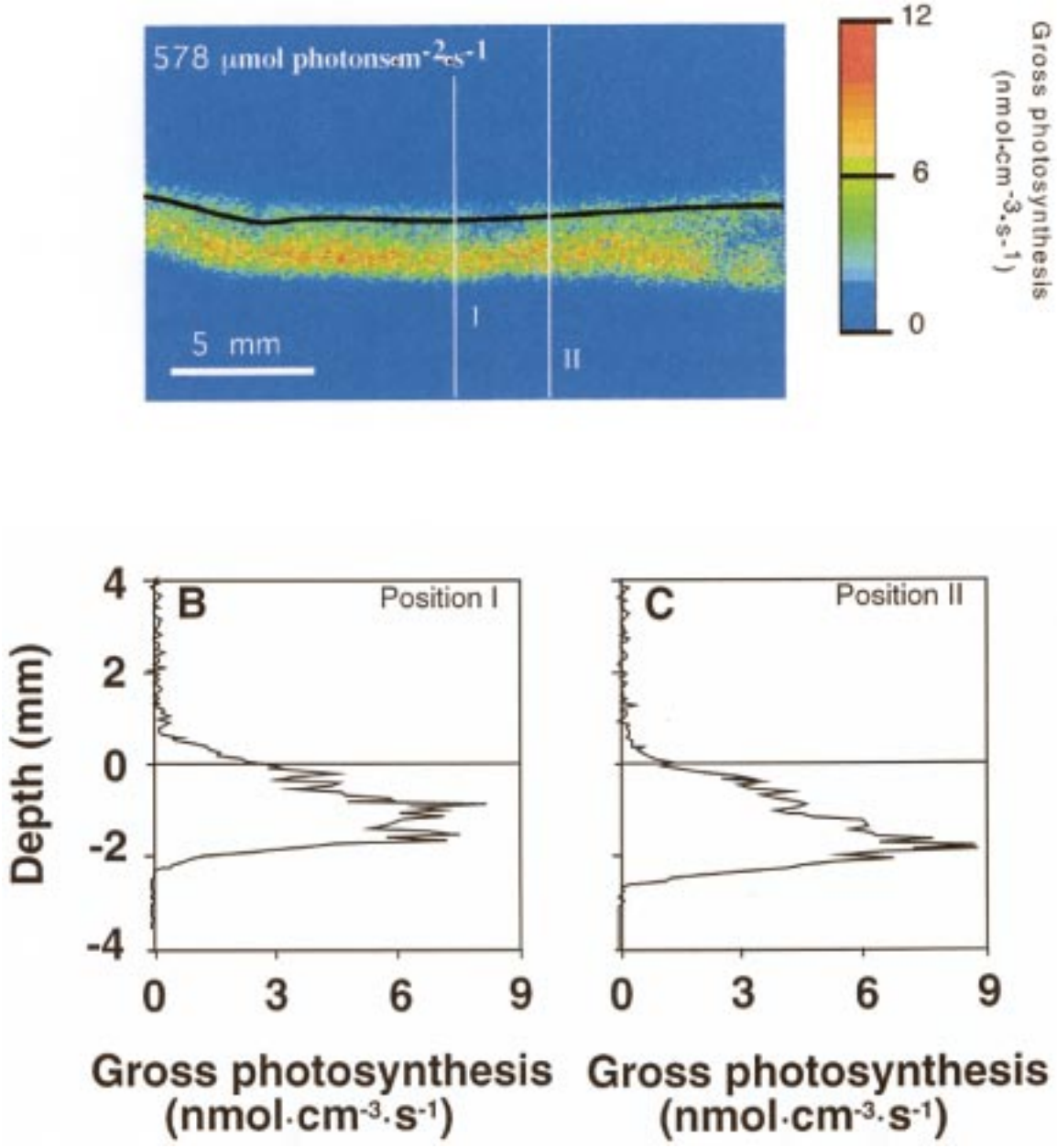


FIG. 7. (A) Gross photosynthetic rates determined by the light–dark-shift technique at an irradiance of 578 µmol photons·$m^{-2}$·$s^{-1}$. The fat horizontal line indicates the position of the mat surface, whereas the two thin vertical lines indicate the position of the profiles shown in panels B and C. Scale bar indicates the physical dimensions.

higher $O_2$ consumption at neighboring consumption sites (Fig. 6). At the highest irradiance, the increase in $O_2$ production was almost completely balanced by increased $O_2$ consumption at the neighboring sites (Fig. 6B). The consumption and production sites most likely reflected areas dominated by heterotrophs and phototrophs, respectively. It has previously been shown that cyanobacteria excrete simple organic photosynthates in light (McFeters et al. 1978), and it has been suggested that enhanced organic carbon leakage from phototrophs during intense photosynthesis could stimulate the activity of the heterotrophs in natural communities (Bauld and Brock 1974, Ward et al. 1987). A strong positive correlation between bacterial production and photosynthetic activity has also been demonstrated in artificial biofilms (Neely and Wetzel 1995). The spatial coupling between consumption and production sites and the light-stimulated respiration within the photic zone strongly suggest a tight coupling between phototrophs and heterotrophs in the investigated natural mat. We hypothesize that this stimulated activity results in an additional supply of inorganic carbon (DIC) for the phototrophs, whereas the $O_2$ concentration is kept relatively low and thereby decreases any photorespiratoric stress.

The high $O_2$ affinity of heterotrophic bacteria with $K_m$ values well below 1 to 3 μM (Hao et al. 1983) makes enhanced respiration due to increased availability of $O_2$ unlikely. The lower rates of net $O_2$ production and consumption within the surface layer, which experienced the highest irradiance, was probably due to a lower cell density. Indeed, the surface layer exhibited a loose structure. In total, we investigated 34 $mm^2$ of oxic zone (three mat samples) at a resolution of 26 μM, and we did not encounter any anoxic microniches at this scale. Microsites (130 × 130 μM) with $O_2$ consumption rates above 4 $nmol \cdot cm^{-3} \cdot s^{-1}$ were encountered only at high light intensities, and they were then surrounded by sites of high net $O_2$ production. No significant difference in dark respiration was noted between the $O_2$ production and $O_2$ consumption sites.

The gross photosynthetic rates of the mat were determined by applying the light–dark-shift technique to the mat (Revsbech and Jørgensen 1983, Glud et al. 1992). As for the net activity, the gross rates reflected a surface layer with low activity and a deeper horizon coinciding with the *Microcoleus* layer with a relatively high activity (Fig. 7). The photosynthetic activity also showed an extensive horizontal variation, with sites characterized by virtually no photosynthesis in the otherwise photic zone (Fig. 7). The 90% response time of the applied planar optode was approximately 3 s, which meant that we had to apply relatively long dark incubations. Because of the diffusion during the requested dark incubation, the activity data were averaged out, resulting in a widening of the $O_2$ production zone into the mat and up into the DBL (Fig. 7). Additionally, the peak activities were underestimated, whereas photosynthesis rates in low-activity zones were overestimated (Glud et al. 1992, Lassen et al. 1998). Therefore, it is difficult to make pixel-to-pixel comparisons between images of the net and gross photosynthesis. However, the integrated gross rates, being independent of the dark incubation period (see Materials and Methods), was 5.2 ± 1.6 $nmol \cdot cm^{-3} \cdot s^{-1}$. The export of $O_2$ from the photic zone as calculated from the flux images (Fig. 2) accounted for only 8% to 10% of the $O_2$ gross production, meaning that approximately 90% of the $O_2$ produced by photosynthesis was consumed within the photic zone. This number is confirmed by the fact that the integrated gross production of $O_2$ was approximately 10 times higher than the integrated net production within the photic zone. To avoid bubble formation during the experiments, our measurements were carried out at relatively low light as compared to the *in situ* daylight conditions. However, any coupling between the heterotrophic and autotrophic activity can be expected to be only tighter at higher irradiances.

Unfortunately, no technique for determining the transport coefficient at a scale relevant for our study exists. Some of the variability we have observed could be ascribed to variability in transport coefficients within the mat. Oxygen transport coefficients as low as 70% of the diffusion coefficient in water have been determined for other microbial mats (Revsbech 1989, Glud et al. 1995). Nevertheless, applying these numbers and the previously observed variability in $D_e(z)$ would not have affected the conclusions made in the present study.

In conclusion, the presented data demonstrate a high variability of $O_2$ concentrations, net activities, and gross photosynthesis of a microbial mat. However, the variability does reflect a tight spatial coupling between $O_2$ producers and consumers, ensuring a highly efficient turnover of solutes within the mat. During light, most of the produced $O_2$ within the photic zone was rapidly consumed within this zone, probably by heterotrophs (and maybe to a smaller degree by photorespiration). Therefore, light clearly stimulated the respiratory potential of the photic zone, and presumably the cycling of DIC between phototrophs and heterotrophs was as tightly coupled as the $O_2$ turnover.

We acknowledge the financial suport from the Max Planck Society (Germany), the European Commission MAST III program (CT970078) (Oliver Kohls), and the Danish Natural Science Research Council (Ronnie N. Glud, Michael Kühl, and Niels B. Ramsing). Eric Epping is thanked for collecting and storing a piece of the microbial mat used in this study.

Bauld, J. & Brock, T. D. 1974. Algal excretion and bacterial assimilation in hot spring algal mats *J. Phycol.* 10:101–6.

Broecker, W. S. & Peng, T. H. 1974. Gas exchange rates between air and sea. *Tellus.* 26:21–35.

Canfield, D. E. & DesMarais, D. J. 1993. Biogeochemical cycles of carbon, sulfur, and free oxygen in a microbial mat. *Geochim. Cosmochim. Acta* 57:3971–84.

Colijn, F. & De Jonge, V. N. 1984. Primary production of microphytobenthos in the EMS-Dollard Estuary. *Mar. Ecol. Prog. Ser.* 14:185–96.

Crank, J. 1983. The mathematics of diffusion. Clarendon Press, Oxford.

Duarte, C. M. & Cebrian, J. 1996. The fate of marine autotrophic production. *Limnol. Oceanogr.* 41:1758–66.

Epping, H. G. & Jørgensen, B. B. 1995. Light enhanced areal oxygen respiration in benthic phototrophic communities. *Mar. Ecol. Prog. Ser.* 139:193–203.

Fenchel, T. 1998. Artificial cyanobacterial mats: cycling of C, O and S. *Aquat. Microb. Ecol.* 14:253–9.

Fenchel, T. & Bernard, C. 1996. Behavioral responses in oxygen gradients of cilliates from microbial mats. *Eur. J. Protistol.* 32: 55–63.

Garcia-Pichel, F., Mechling, M. & Castenholz, R. W. 1994. Diel migrations of microorganisms in a hypersaline microbial mat. *Appl. Environ. Microbiol.* 60:1500–11.

Glud, R. N, Gundersen, J. K., Revsbech, N. P. & Jørgensen B. B. 1994. Effects on the benthic diffusive boundary layer imposed by microelectrodes. *Limnol. Oceanogr.* 39:462–7.

Glud, R. N., Jensen, K. & Revsbech N. P. 1995. Diffusivity in surficial sediments and benthic mats determined by use of a combined $N_2O$-$O_2$ microsensor. *Geochim. Cosmochim. Acta* 59: 231–37.

Glud, R. N. Ramsing, N. B., Gundersen J. K. & Klimant I. 1996. Planar optrodes, a new tool for fine scale measurements of two dimensional $O_2$ distribution in benthic communities. *Mar. Ecol. Prog. Ser.* 140:217–26.

Glud, R. N., Ramsing, N. B. & Revsbech, N. P. 1992. Photosyn-

thesis and photosynthesis coupled respiration in natural biofilms quantified with oxygen microelectrodes. *J. Phycol.* 28: 51–60.

Glud, R. N., Santegoeds, C. M., de Beer, D., Kohls O. & Ramsing N. B. 1998. Oxygen dynamics at the base of a biofilm studied with planar optrodes. *Aquat. Microb. Ecol.* 14:223–33.

Hao, O. J., Richard, M. G. & Jenkins, D. 1983. The half saturation coefficient for dissolved oxygen: a dynamic method for its determination and its effect on dual species competition. *Biotechnol. Bioeng.* 25:403–16.

Jørgensen, B. B. & DesMarais, D. J. 1990. The diffusive boundary layer of sediments: oxygen microgradients over a microbial mat. *Limnol. Oceanogr.* 35:1343–55.

Jørgensen, B. B. & Revsbech, N. P. 1985. Diffusive boundary layers and the oxygen uptake of sediments and detritus. *Limnol. Oceanogr.* 30:111–22.

Jørgensen, B.B., Revsbech, N. P. & Cohen Y. 1983. Photosynthesis and structure of benthic microbial mats: microelectrode and SEM studies of four cyanobacterial communities. *Limnol. Oceanogr.* 28:1075–93.

Kautsky, H. 1939. Quenching of luminescence by oxygen. *Trans. Faraday Soc.* 35:216–9.

Klimant, I., Meyer, V. & Kühl M. 1995. Fiber-optic oxygen microsensors, a new tool in aquatic biology. *Limnol. Oceanogr.* 40: 1159–65.

Kühl, M., Glud R. N., Ploug, H. & Ramsing, N. B. 1996. Microenvironmental control of photosynthesis and photosynthesis-coupled respiration in an epilithic cyanobacterial biofilm. *J. Phycol.* 32:799–812.

Lassen, C. Glud R. N., Ramsing, N. B. & Revsbech N. P. 1998. A method to improve the spatial resolution of photosynthetic rates obtained by oxygen microsensors. *J. Phycol.* 34:89–93.

Li, Y. H. & Gregory, S. 1974. Diffusion of ions in deep-sea sediments. *Geochim. Cosmochim. Acta* 38:703–14.

Ludden, E., Admiraal, W. & Colijn, F. 1985. Cycling of carbon and oxygen in layers of marine microphytes: a simulation model and its eco-physiological implications. *Oecologia* 66:50–9.

McFeters, G. A., Stuart, S. A. & Olson, S. B. 1978. Growth of heterotrophic bacteria and algal extracellular products in oligotrophic waters. *Appl. Environ. Microbiol.* 35:383–91.

Neely, R. K. & Wetzel, R. G. 1995. Simultaneous use of $^{14}C$ and $^{3}H$ to determine autotrophic production and bacterial production in periphyton. *Microb. Ecol.* 30:227–37.

Revsbech, N. P. & Jørgensen B. B. 1983. Photosynthesis of benthic microflora measured by the oxygen microprofile method: capabilities and limitations of the method. *Limnol. Oceanogr.* 28: 749–56.

Revsbech, N. P., Jørgensen, B. B., Blackburn, T. H. & Cohen, Y. 1983. Microelectrode studies of the photosynthesis and $O_2$, $H_2S$, and pH profiles of a microbial mat. *Limnol. Oceanogr.* 28:1062–74.

Revsbech, N. P., Jørgensen, B. B. & Brix, O. 1981. Primary production of microalgae in sediments measured by oxygen microprofile, $H^{14}CO_3^-$ fixation and oxygen exchange methods. *Limnol. Oceanogr.* 26:717–30.

Stern, O. & Volmer, M. 1919. Uber die Abklingzeit der Fluoreszenz. *Phys. Z.* 20:183–8.

Ward, D. M., Tayne, T. A., Anderson, K. L. & Bateson, M. M. 1987. Community structure and interactions among community members in hot spring cyanobacterial mats. *In* Fletcher, M., Gray, T. R. S. & Jones, J. G. [Eds.] *Ecology of Microbial Communities.* Cambridge University Press, Cambridge, pp. 179–210.